A Molecular Dynamics Study of a Model Nanoparticle Embedded in a Polymer Matrix

D. Brown,* P. Mélé, S. Marceau, and N. D. Albérola

Laboratoire Matériaux Organiques à Propriétés Spécifiques (LMOPS), UMR 5041 Université de Savoie−CNRS, Campus Sciéntifique, 73376 Le Bourget-du-Lac, France

Received June 17, 2002

ABSTRACT: Molecular dynamics (MD) simulations have been used to examine the structure and dynamics of a system containing an inorganic nanoparticle embedded in a polymer matrix. This paper represents a preliminary investigation into the feasibility of examining such relatively large systems using atomistic modeling techniques. No attempt is made here to model any specific system. A generic linear polymer "united-atom" model is first created in an amorphous phase before the insertion of an atomistically detailed silica nanoparticle of diameter ∼4.4 nm. A novel method to insert a nanoparticle into a polymer matrix is given. The entire system is contained in a standard periodic simulation cell of side length ∼10 nm. The volume fraction of silica corresponded to ∼4.5%. The composite system was subsequently relaxed at 300 K and at two different pressures using standard MD techniques, the *gmq* suite of programs being used for this purpose. Results are presented regarding the variation of the structure and dynamics of the system with respect to the distance from the polymer−nanoparticle interface and as a function of pressure. A clear structuring of the polymer chains around the nanoparticle is seen with prominent first and second peaks in the radial density function and a concurrent development of preferred chain orientation. The probability of trans conformers is also higher close to the interface and shows a distinct gradient. In contrast, evidence for chain immobilization is less obvious overall although dynamic properties are more sensitive to changes in the pressure. Comparisons are also made between the bulk moduli of the pure polymer and composite systems.

1. Introduction

The mechanical behavior of heterogeneous polymer systems is governed, at the mesoscopic scale, by the effects of mechanical coupling between phases and, at the molecular level, by the modifications of molecular mobility in the polymer matrix chains by the interactions at the polymer−inclusion interface.[1−9] The contribution to the reinforcement effect of the polymer matrix by the inclusions (or mechanical coupling) is governed, in particular, by the distribution of the size of the phases, which is often difficult to determine experimentally. In effect, the interactions at the interfaces and the mechanical coupling can lead to similar modifications of the viscoelastic behavior.[2]

In the case of systems reinforced by inclusions of submicronic size, the intensity of the mechanical coupling and the amplitude of the effects linked to the interfacial interactions increase as the size of the inclusions diminish or if the structure becomes more complex.[10−13]

At the mesoscopic scale, the mechanical coupling between the phases in the heterophase systems depends, thus, on not only the properties and relative volume fractions of each but also the geometry of the reinforcing component and the architecture of the material, in other words, the relative spatial distribution of the phases present.[14−16] For a given volume fraction of submicronic inclusions, the distances between inclusions in the polymer matrix diminish drastically, increasing the probability of the formation of aggregates and leading generally to a separation of the phases into independent connectivities or co-continuous.[17,18] The percolation threshold of these particles will be thus more affected by their geometric form and structure.[19]

At the molecular level, the influence of interactions at the polymer−reinforcement interface on the molecular mobility and structure of neighboring chains is amplified in the case of objects of small dimensions in a more or less complex way, because the relative amount of material in the vicinity of the interface is inversely proportional to the size of the inclusions. Thus, although experimental work[20,21] points to a reduction in molecular mobility in the region of the interface, little is known about the origin of this immobilization, the possible accompanying changes in structure or the spatial extent of these two effects.

For the above reasons it is interesting to undertake a study of such a system using a molecular modeling approach. The structure and dynamics of the nanoparticle−polymer matrix interface have only recently started to become studied using such simulation techniques[22−26] although the structure and dynamics of polymers at plain and other interfaces have been studied for some time. Bitsanis et al.[27] give a review of some of the early work in the field and describe their molecular dynamics simulations of liquid systems of relatively short freely jointed chains in the vicinity of a plain wall. More recently, Binder and co-workers have used dynamic Monte Carlo simulations using the bond-fluctuation lattice model to study similar systems using an even more coarse-grained approach.[28,29] This group has also modeled the polymer−fiber interface in a model composite using the same techniques.[30] We note also that there have been recent developments in the related field of nanocolloidal systems where expanded ensemble Monte Carlo methods have been applied to the problem of obtaining the chemical potential of hard particles inserted into dilute hard-sphere polymer solutions.[31]

* To whom correspondence should be addressed. E-mail: David.Brown@univ-savoie.fr.

10.1021/ma020951s CCC: $25.00
Published on Web 01/18/2003

This technique seems potentially useful with regard to certain questions concerning the thermodynamics of mixing of nanoparticles and polymer matrices.

One of the major problems for atomistic level simulations is that the time and length scales accessible are restricted by the computing power available. Thus, many technologically interesting systems which extend over large distances and/or relax on long time scales are difficult to simulate adequately. The advent of parallel processing, on the other hand, has resulted in an unprecedented increase in the available processing power which, if it can be harnessed efficiently, offers the prospect of being able to simulate larger more complicated systems with slower molecular processes. Over the past few years significant developments have been made in the mapping of general MD algorithms to parallel processors within a domain decomposition framework.[32,33] Concurrent with this has been the development of a general purpose parallel MD code, called *ddgmq*,[34] and it is this program which will be eventually used to tackle these computationally demanding problems.

In this paper results are presented of a pilot study of a model polymer matrix reinforced by a mineral nanoparticle. Unlike previous similar studies,[22−25] the nanoparticle is modeled with atomistic detail. Among other things, this added detail allows us to determine the mechanical properties of the bulk reinforcing phase in order to make connections with micromechanical modeling.

This preliminary project is designed to probe the feasibility and the possible insights that can be gained before attempting a subsequent more detailed study using more intensively the parallel MD techniques alluded to above. The process of simply incorporating a nanoparticle into a polymer matrix raises in itself a fundamental question for the molecular modeler as to how this can be done in a way which best avoids artifacts. It has to be emphasized that relaxation times in polymers can exceed by many orders of magnitude the time scale available to MD simulations. Systems thus have to be constructed as close as possible to a relaxed state as otherwise the system will be forever changing in the subsequent dynamic simulation.[35,36] For this reason techniques for overcoming the incorporation problem are best tested on simpler models in which all the essential features can be included but at a much lower computational cost. Once a relaxed system is obtained, the simpler model can also be used to examine the degree of structural and dynamic changes introduced into the system by the presence of a nanoparticle. The model will give a good idea of the intensity of these changes and what the statistically significant level of resolution is likely to be for more detailed models of a similar size.

This and subsequent MD studies will form an integral part of a wider ranging strategic and fundamental project concerning the fabrication and characterization of nanocomposites. This project will create real samples of nanocomposites in the best possible conditions for subsequent scientific analysis by dynamic mechanic methods, NMR, X-ray diffraction, electron microscopy, etc., and use all this information to refine micromechanical models designed to describe the mechanical response of the system to applied deformations.[37,38] Ideally, this nanocomposite would be a system of perfectly spherical nanoparticles, all of exactly the same size, distributed homogeneously in a completely amorphous polymer matrix constructed from a relatively uncomplicated homopolymer. Of course, in reality the experimentalist has many difficulties attaining this ideal; monodisperse powders of nonaggregating nanoparticles are not readily available, for example, and the practicalities of dispersing the particles homogeneously in the polymer matrix often implies certain complicating factors, such as the addition of coupling agents.

Table 1. Parameters for the Buckingham Potential (Eq 1) for the Atom Types Given

atom type 1	atom type 2	*A*/eV	*B*/Å	*C*/eV Å^6
Si	Si	872 360 000	0.065 70	23.300
Si	O	10 722	0.208 51	70.735
O	O	1756.9	0.351 32	214.74
CH_2	CH_2	4 208 000	0.208 29	0
CH_2	Si	60 588 000	0.137 00	0
CH_2	O	85 982	0.279 81	0

The primary goal is simply to assess whether new parallel domain decomposition molecular dynamics algorithms can be used to efficiently simulate such systems and whether useful information can be extracted regarding the polymer matrix−nanoparticle interface and the mechanical reinforcement effects.

2. Details of the Simulations

2.1. The Model Silica Nanoparticle. As our eventual aim will be to look at systems containing silica nanoparticles, this initial study has used a relatively detailed model nanoparticle made up of Si and O atoms. This is in distinction to recent simulations which have either used a single large smooth sphere[22,23] or icosohedral shells of atoms[24] to represent the inclusions. Atomistic models of the structure of amorphous silica can be quite complicated, however, and often involve "three-body" terms; i.e., angle bending potentials are used for certain O···Si···O triplets depending on the O···Si distances.[39] For the purpose of testing the general approach a simpler model can be used, and so the model of Tsuneyuki[40] of crystalline polymorphs of silica has been chosen. It has already been shown to reproduce surprisingly well the structures of a number of crystalline polymorphs of silica, given the fact that these structures differ in density from ∼2.3 g cm^{-3} (low cristobalite) to as much as 4.3 g cm^{-3} (stishovite) and in bulk moduli from 18 to 300 GPa. The model is relatively straightforward consisting of just two-body interactions; a Buckingham (exponential-6) potential represents the van der Waals interactions

$$\Phi_{vdw}(|\mathbf{r}_{ij}|) = A \exp(-|\mathbf{r}_{ij}|/B) - C|\mathbf{r}_{ij}|^{-6} \qquad (1)$$

and partial charges are placed on each atom ($q_{Si} = 2.4e$, $q_O = -1.2e$) to describe the Coulombic interactions. Values of the parameters for each type of pair interaction are given in Table 1.

To test the model of Tsuneyuki, some MD simulations have been carried out. Starting from the crystal structure of α-quartz, a system of 1125 atoms, i.e., a supercell of 5 × 5 × 5 unit cells, was first equilibrated at 300 K at a pressure of 1 bar for a period of 200 ps. A production simulation was then carried out for a further 300 ps. This MD simulation was performed using the *gmq* MD program[34] running on an SGI O2 workstation. The time step used was 5 fs, and each time step took about 0.92 s of CPU time. The average temperature was kept close

Table 2. A Comparison of the Results Obtained Here for α-Quartz with Those Obtained Previously Using the Tsuneyuki Model and Experiment[a]

	MD (this work)	MD[b]	exp[c]
a/Å	5.0143 ± 0.0002	5.02	4.916
b/Å	5.0144 ± 0.0002	5.02	4.916
c/Å	5.5450 ± 0.0002	5.55	5.4054
α/deg	90.003 ± 0.004	90	90
β/deg	89.996 ± 0.004	90	90
χ/deg	120.003 ± 0.004	120	120
density/kg m^{-3}	2479.1 ± 0.1	2470	2645.8
E/GPa	82 ± 3		
K_o/GPa	32 ± 1	33.7	38 ± 3

[a] We point out that the work described here used a 5 × 5 × 5 unit cell model (1125 atoms) whereas Tsuneyuki's system was smaller, 4 × 4 × 4 unit cells (576 atoms). [b] From the work of Tsuneyuki.[40] [c] From the work of Levien et al.[45]

to 300 K using the loose-coupling method of Berendsen et al.[41] with a τ_T of 0.1 ps. The average on- and off-diagonal components of the pressure tensor were maintained close to their required values of 1 bar and zero, respectively, using a loose-coupling method[42] with a τ_P of 10 ps.[34] The truncation radius for Buckingham and for the real-space part of the electrostatic potential interactions, R_c, was set throughout at half the minimum perpendicular distance between any two opposite faces of the periodic MD box and thus varied with time. Long-range corrections to the energy and the pressure were made on the assumption that $g(r) = 1$ beyond the cutoff. Optimum convergence of the Ewald sum[43] was obtained by using a separation parameter $\alpha = 0.36$ Å^{-1} and a reciprocal space cutoff $K_{max} = 12$. These values give convergence of the direct and indirect routes to the reciprocal space part of the Ewald sum contribution to the pressure of better than 10 bar.[44]

The average unit cell parameters and density obtained from the 300 ps production simulation after equilibration at 300 K are compared to the values obtained previously by MD[40] and the experimental values[45] in Table 2. There is a good agreement between the two MD simulations carried out using the same potential. The small differences can probably be attributed to the fact that the system sizes are not the same (see Table 2). As reported previously, the model reproduces the symmetry of α-quartz although errors in the cell lengths are 2−3%.[40]

To obtain some information about the elastic moduli of the model, further simulations were carried out. First, starting from the equilibrated structure, a uniaxial extension experiment[46] was performed with the tension being applied along the *c*-axis of the crystal. The required tension in this direction was gradually increased at a rate of 10 bar/ps up to a value of 3000 bar. The resulting extension vs measured tension plot (not shown) was quite linear, and a least-squares fit of the data gave a Young's modulus in this direction of around ∼82 GPa.

To obtain the bulk modulus, further equilibrium simulations were carried out at a higher density ($p \sim$ 3000 bar) and a lower density ($p \sim -1000$ bar). The density vs pressure data for all three equilibrium points were found to lie on the same straight line (plot not shown). From the definition of the compressibility, $\beta = -(1/V)(dV/dP) = (1/\rho)(d\rho/dP)$, the slope of the density vs pressure plot ($d\rho/dP = 0.00763$ kg m^{-3} bar^{-1}), and the density at a pressure of 1 bar ($\rho = 2479.1 \pm 0.1$ kg m^{-3}) a value for β is obtained of $\sim 3.1 \times 10^{-6}$ bar^{-1}. This in turn gives for the bulk modulus, $K_0 = -V(dP/dV) = 1/\beta$, an estimate of ∼32 GPa, which is close to the value obtained previously by Tsuneyuki (see Table 2). Although the experimental value is somewhat higher at 38 GPa, for our purposes in this paper the model is adequate in that it has elastic moduli in the right order of magnitude, i.e., substantially higher than those in an amorphous polymer matrix.

Having established the adequacy of the Tsuneyuki model, the next step was to create a roughly spherical nanoparticle for later insertion into the model polymer matrix. To do this, an α-quartz supercell crystal structure was first created, and then all Si and O atoms outside a radius of ∼20 Å from the center were discarded. The resulting cluster contained 914 Si atoms and 1828 O atoms and was thus electrically neutral. For this feasibility study the use of a starting crystalline configuration rather than an amorphous phase of silica is of no consequence. The subsequent problem of embedding this nanoparticle in a polymer matrix and relaxing the system is the same.

2.2. The Model Polymer Matrix. The model polymer matrix used in this study is based on one which has been often employed to study amorphous polymer systems.[35,46−48] In this model, linear chains of *n* united-atom CH_2 sites are held together by rigid bonds, and a valence angle and torsion angle potentials give internal structure and rotational barriers. Nonbonded interactions are represented by a purely repulsive potential which operates for all intermolecular pair interactions and between all pairs of sites in the same chain separated by at least three intervening ones. In the original model this latter potential took the form of a Lennard-Jones (LJ) 12−6 potential truncated at the minimum and raised by the well depth to give a repulsive potential smoothly decaying to zero, often referred to as a Weeks−Chandler−Andersen, or WCA, potential. In this case the WCA potential is replaced by the Buckingham form so as to facilitate the interactions with the Si and O atoms. As only a repulsive interaction is required for nonbonded site−site interactions, the potential took the form of eq 1 with the constant *C* set to zero. The two adjustable constants, *A* and *B*, were obtained from nonlinear least-squares regression fits to the original WCA form in the range from 3.9 to 4.8 Å, which corresponds to the important region of nearest-neighbor interactions. The resulting best-fit parameters are shown in Table 1 and were found to lead to a good correspondence with the WCA model.

For the purpose of this study one long chain of $n =$ 30 000 sites was constructed using a generation technique[35] known to produce representative configurations from the dense amorphous phase.[48] In an initial sampling phase the chain is subject to pivot Monte Carlo moves for bond angles and dihedral angles in which nonbonded interactions are restricted to just those atoms separated by three others along the chain; all other nonbonded interactions being ignored. In a second stage the nonbonded interactions ignored in the first phase are smoothly introduced. The resulting model polymer matrix formed is thus one in which one single chain gives a dense system through the replicative properties of the periodic boundary conditions. This system was subsequently relaxed using molecular dynamics for 1000 ps at a temperature of 300 K under constant isotropic pressure conditions; i.e., the MD box is constrained to remain cubic, using a loose-coupling method[42] with a τ_P of 2 ps.[34] To compensate for the lack

of attractions, an overpressure of 5000 bar was applied; this results in relaxed densities which correspond closely to those found if attractions are included in the nonbonded potential and atmospheric pressure is applied. To account for the high-frequency motions in the intramolecular modes of the polymer, a smaller time step of 2 fs was employed. The configuration at the end of this period of 1000 ps was then used as the starting point for the insertion of the silica nanoparticle (see next section).

Subsequently, the simulation of the matrix was continued under conditions of constant pressure tensor, all cell lengths and angles free to vary independently, first at an applied pressure of 5000 bar and subsequently at an applied pressure of 4630 bar. In both cases this was to produce results for the matrix alone for comparison with those generated for the same conditions for the composite (see following section). Both these extra simulations were carried out for a total of 1000 ps each.

2.3. The Model Composite. Bringing together the nanoparticle with the matrix raises an interesting fundamental question concerning the state of polymer chains in composite systems. Previous similar studies[22−25] have used relatively short chain lengths whose global configurations could be more or less equilibrated within the duration of the simulation. In keeping with our eventual comparison with a real composite system, the chain length used here was much higher, and so the brute force approach is not an option, even if it was desired. An alternative approach would be to perform the initial sampling phase of the matrix construction in the presence of polymer−inclusion interactions; in fact, the polymer would have to interact with an ordered 3D array of inclusions because of the periodicity of the simulation box. Indeed, recent work on exactly this problem suggests that the equilibrium distribution of configurations for $n = 300$ chains in such a 3D array of nanoparticles is different from that in the corresponding pure polymer.[49] However, we point out that the single chain sampling technique of Sharaf et al.[49] has been called into question in this respect[50] as it leads to distributions consistent with dilute polymer solutions rather than dense melts. Nevertheless, the work of Vacatello[50] confirms that the equilibrium distribution of $n = 100$ chains in a filled system differs from that in the pure melt.

The practical problems aside, this method was discarded on the grounds that this perturbation did not correspond to our initial preconception of the composite forming process. It has to be said, however, that experimentally the polymer chain configurations will depend very much on the method of preparation of the composite, and certainly in some cases this can lead to a distribution far from a global equilibrium, e.g., if the composite is fabricated using latex.[51,52] In this paper the nanoparticles are considered as being mechanically mixed into an existing equilibrium melt of very high viscosity, i.e., configurational relaxation times much longer than mixing times, and thus lead to a minimum of perturbation. With this in mind two methods were tested.

The first was simply to superimpose the two systems and then let the energy minimizer do the job of separating the two components. This was tried but a large disruption of the inclusion resulted, and so this method was quickly discarded. Ultimately, it was found preferable to first create and relax the polymer matrix and then create a cavity of the appropriate size before inserting the desired inclusion. The cavity was first created in the already prepared relaxed polymer matrix (see previous section) using a soft repulsive potential[34] of the following form

$$\Phi_{\mathrm{cav}}(\mathbf{r}_i) = \frac{1}{2}k_{\mathrm{cav}}(|\mathbf{r}_i - \mathbf{R}_{\mathrm{o}}| - r_{\mathrm{cav}})^2 \quad \text{for } |\mathbf{r}_i - \mathbf{R}_{\mathrm{o}}| < r_{\mathrm{cav}} \tag{2}$$

where k_{cav} is a force constant (in this case 50 kg s^{-2}), $\mathbf{r}_i$ is the current position vector of atom i, $\mathbf{R}_{\mathrm{o}}$ is the position vector of the origin of the center of the cavity (in this case the center of the MD box), and r_{cav} is the current radius of the cavity. By restricting the interaction to just particles which fall within the cavity, we have one side of a harmonic potential which gives a smoothly decaying soft repulsive wall. To avoid problems when starting to inflate the cavity, the forces that originate from this potential are limited by an upper bound which corresponds to a maximum displacement in one time step of 0.1 Å. By increasing linearly r_{cav} from zero to a value large enough to accept the silica particle over a period of time, disruption of the carefully prepared polymer matrix was minimized. To avoid a densification of the polymer matrix, the MD box was also slightly expanded by an amount sufficient to compensate for the volume excluded to it at the center. The nanoparticle was then inserted into the spherical cavity and the soft wall potential switched off. Cross interactions between the polymer and the silica were described using standard combining rules, $A_{IJ} = (A_{II}A_{JJ})^{1/2}$, $B_{IJ} = (B_{II} + B_{JJ})/2$, and $C_{IJ} = (C_{II}C_{JJ})^{1/2}$, and were thus completely repulsive in nature. The actual values are also shown in Table 1.

For the MD simulations of the 32 742-atom composite system the time step was maintained at 2 fs, as for the polymer alone. The parameters for the Ewald sum were retuned to take account of the change in the box size. A reasonable compromise between precision and cost was obtained with $\alpha = 0.17$ Å^{-1}, $K_{\mathrm{max}} = 8$, and $R_{\mathrm{c}} = 12$ Å. The same 12 Å truncation was also used for Buckingham interactions which contained a nonzero attractive part, i.e., those with $C \neq 0$ in Table 1, and long-range corrections to the energy and pressure were calculated using $g(r) = 1$ beyond this value.

For those atom pairs subject to purely repulsive Buckingham interactions, i.e., those with $C = 0$ in Table 1, shorter truncation distances were used for each type of pair interaction concerned based on a lower bound for the energy of interaction, E_{c},

$$R_{\mathrm{c}IJ} = -\ln(E_{\mathrm{c}}/A_{IJ})B_{IJ} \tag{3}$$

A value of E_{c} equivalent to Boltzmann's constant multiplied by a temperature of 0.1 K was found to lead to negligible differences in the evaluated energies.

The combined nanoparticle−matrix system was first relaxed for 2000 ps under constant volume conditions with the average temperature being kept close to 300 K using the loose-coupling method of Berendsen et al.[41] with a τ_{T} of 10 ps. During this period the average isotropic pressure was found to stabilize at ∼4630 bar, but the restriction of a cubic box gave rise to slight differences between the on-diagonal components of the pressure tensor and also off-diagonal components which were marginally nonzero—a common problem for atomistic simulations of systems in the solid state. To relax

Table 3. Average Properties from the Simulations of the Pure Matrix and the Composite Systems at 300 K and the Pressures Given[a]

	matrix, $P = 4630$ bar	composite, $P = 4630$ bar	matrix, $P = 5000$ bar	composite, $P = 5000$ bar
total energy	6936 ± 2	-148308 ± 2	7022 ± 4	-148256 ± 2
bending energy	1248 ± 1	1255 ± 1	1250 ± 1	1253 ± 1
torsion energy	2121 ± 2	2089 ± 1	2142 ± 2	2101 ± 1
vdW energy	1074 ± 1	8613 ± 2	1137 ± 2	8663 ± 1
$SiO_2 \cdots SiO_2$		7460 ± 2		7462 ± 2
$CH_2 \cdots SiO_2$		29.3 ± 0.4		30.2 ± 0.4
$CH_2 \cdots CH_2$	1074 ± 1	1124 ± 1	1137 ± 2	1171 ± 1
coulombic energy		-163099 ± 2		-163107 ± 2
density/kg m^{-3}	757.2 ± 0.2	815.7 ± 0.2	764.8 ± 0.2	824.8 ± 0.1
vol/Å^3	922825 ± 210	968411 ± 140	913691 ± 210	957781 ± 110
a/Å	96.37 ± 0.03	98.3 ± 0.1	96.20 ± 0.03	96.95 ± 0.03
b/Å	98.58 ± 0.03	100.2 ± 0.2	97.94 ± 0.05	100.97 ± 0.02
c/Å	97.18 ± 0.04	98.3 ± 0.1	97.01 ± 0.03	97.88 ± 0.02
α/deg	90.45 ± 0.05	90.03 ± 0.03	90.17 ± 0.04	90.24 ± 0.05
β/deg	89.19 ± 0.05	89.32 ± 0.07	89.49 ± 0.04	88.66 ± 0.02
γ/deg	91.53 ± 0.03	90.33 ± 0.06	91.44 ± 0.03	90.63 ± 0.01
volume fraction of SiO_2/%		~ 4.42		~ 4.47
% *trans*	83.9 ± 0.1	85.2 ± 0.1	83.6 ± 0.1	84.9 ± 0.1

[a] All averages were taken over the last 500 ps of each simulation. Average energies are quoted in J/mol of CH_2 sites.

out the inequalities in the on-diagonal components and to allow the off-diagonal components to go to zero, the simulation was switched to NPT conditions where the average on- and off-diagonal components of the pressure tensor were maintained close to their required values of 4630 bar and zero, respectively, using a loose-coupling method[42] with a τ_P of 2 ps.[34] After a further 500 ps the required pressure was set to 5000 bar, and the simulation continued for a further 1000 ps.

The simulations of the composite system were mostly carried out using the general purpose parallel MD program *ddgmq*[32−34] running on 27 processors either on the Cray T3E at IDRIS (Orsay, France) or the SGi Origin 2000 at CINES (Orsay, France). Further simulations were carried out locally using the scalar version of the code, *gmq*, on SGi O2 workstations and a COMPAQ DS20E biprocessor server. In the present implementation of our parallel MD code, it is the largest cutoff in real space, in this case 12 Å, which controls the extent to which the system can be decomposed and thus the maximum number of processors that can be used. This limitation arises as communications are currently restricted to those between nearest-neighbor domains.[32] We would like to point out that, in this particular case, using potentials containing attractive terms, and thus of longer range, for the chain−chain and chain−nanoparticle interactions would have changed neither the maximum number of processors that could have been used nor the efficiency for a given number of processors.

3. Results and Discussion

3.1. Thermodynamic Data. The averages of various thermodynamic properties are given in Table 3 for the simulations of the pure matrix and the composite systems at 300 K, the columns being labeled according to the applied isotropic pressure. Averages were taken over the last 500 ps of each simulation. The total potential energy has been resolved into its components parts in Table 3 in order to see the underlying variations. All energies are quoted in J/mol of CH_2 sites so as have a common normalizing factor.

For the stiff modes in the system, the angle bending part of the polymer intramolecular energy and the intermolecular silica−silica interactions, there is very little variation in their corresponding energies, as would be expected. Silica has significantly higher moduli than the polymer matrix, and thus the particle deforms much less when the pressure is raised. In the polymer matrix changes in the structure, either due to inclusion of the particle or by the increased pressure, manifest themselves principally in changes in the torsion and van der Waals energies. Inclusion of the nanoparticle is accompanied by a decrease in the torsion energy and an increase in the VdW energy of the matrix. The net decrease in torsion energy is consistent with the corresponding increase in the proportion of trans conformers, the averages for which are also given in Table 3. It will be shown later that there is a spatial dependence to this inclusion-induced change in polymer structure.

Also shown in Table 3 are the mean densities, volumes, cell lengths, and cell angles for the four relaxed systems. The changes induced in the volume by the applied pressure will be discussed in a later section concerning the bulk moduli. The deviations of the MD cell lengths and angles from a perfectly cubic shape are not unusual for systems of this size. They reflect the large pressure fluctuations which are concomitant with a relatively small volume, the two being inversely proportional.

3.2. Molecular Structure. In this section we concentrate on the changes induced in the structure of the polymer matrix by the inclusion of the silica nanoparticle. As the nanoparticle is highly spherical, the spatial variation of the polymer structure and mobility have been analyzed simply with respect to the distance, *R*, from the center-of-mass of the silica nanoparticle to a CH_2 site. The histograms to be presented have been accumulated with respect to *R* and by averaging over the last 500 ps of the simulation.

3.2.1. Mass Distribution. In Figure 1 the mass density of polymer as a function of *R* is presented for the composite system simulated at the two pressures. A resolution of 0.1 Å was used for the accumulation of this histogram. Although the largest inscribable sphere in the simulation box has a radius of ∼50 Å, data were obtained out to larger distances by accumulating the histograms into the corners of the box and then normalizing by the volume of the truncated spherical shells. The volumes of these truncated spherical shells beyond

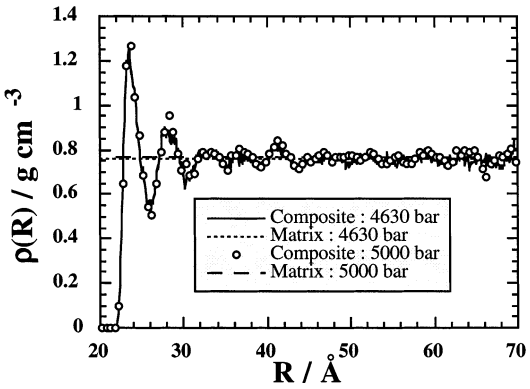

Figure 1. Mass density of the polymer as a function of R, the distance from the center-of-mass of the silica particle. The dotted and dashed lines give the limiting, large R, densities as determined from the pure polymer matrix simulations at the pressures shown.

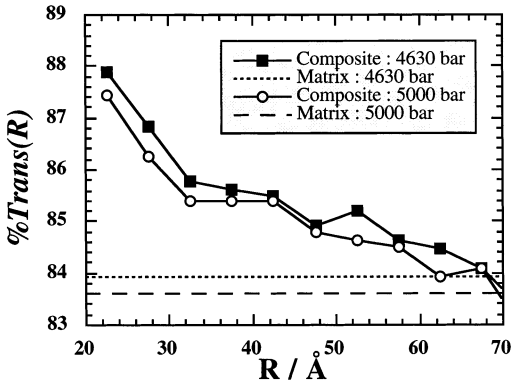

Figure 2. Mean percentage of *trans* conformers plotted as a function of R. The dotted and dashed lines give the limiting, large R, *% trans* as determined from the pure polymer matrix simulations at the pressures shown.

∼50 Å obviously diminish, but at 70 Å the shell volume is similar to that at ∼20 Å and thus has a similar statistical significance.

Figure 1 shows that the polymer is completely excluded from the space up to $R \sim 22$ Å occupied by the silica, but then distinct first and second shells of polymer are then evident with a width of ∼4 Å, very similar to that seen before for chains in the presence of plain walls (see the work of Bitsanis et al.[27] and references therein) and nanocomposites.[22,24] Although less evident, the third, fourth, and fifth peaks follow at similar intervals. The comparison between the results for the two pressures shows that this structure persists at least within the time scale of the simulation. At larger distances the density must tend to that found in the pure polymer matrix at the same applied pressure. These values are indicated by the straight lines in Figure 1.

3.2.2. Conformer Distribution. The average percentages of backbone −C−C−C−C− trans conformers were given for each simulation in Table 3. The inclusion of the nanoparticle leads in both cases to an increase in the *% trans* of ∼1.3%, indicating a certain change induced in the conformations of chains. To put this change into perspective, it can be seen that an increase in pressure from 4630 to 5000 bar has the opposite effect of reducing the *% trans* by about 0.3%. To spatially resolve the changes induced in the conformations, the *% trans* has been calculated as a function of R, and the results are presented in Figure 2. The histograms shown were accumulated using a bin width of 5 Å. Torsions were assigned to the bins according to the value of R for the position of the second atom in the torsion. Values of *% trans*(R) for R greater than ∼50 Å, i.e., half the box length, were also obtained by accumulating statistics into the corners of the box. In principle, we could extend the range of R to $\sim 50\sqrt{3}$ Å, but increasingly poorer statistics, due to the decreasing number of atoms at larger R, render values above ∼70 Å unreliable and are not shown.

Figure 2 reveals that there is a significant increase in the *% trans* in the region close to the nanoparticle. It also confirms the previous result that the influence of the nanoparticle extends to at least 30−40 Å beyond the actual interface. Differences between the results at the two applied pressures show that the diminution in the *% trans* with pressure is spatially homogeneous in the composite system.

Histograms with a higher resolution of 0.1 Å, i.e., as for the mass density, are subject to significant amounts of statistical fluctuations and are not shown. However, they do suggest a correlation between the peaks in density and those in *% trans*. Indeed, there is a peak in the *% trans*(R) at ∼23 Å, corresponding to the position of the first peak in $\rho(R)$, of over 90%.

3.2.3. Alignment Distribution. To further characterize the structure induced in the polymer matrix by the presence of the nanoparticle, the alignment of chains with respect to the interface has been calculated as a function of R. To do this, we consider each consecutive triplet of CH_2 sites on the chain $\{i,j,k\}$. The angle, θ, is then defined as that between the vector from the center of mass of the nanoparticle to particle j and the vector between particles i and k. In effect, θ is the angle between the outwardly pointing vector normal to the interface and the local axis of the polymer chain. The first two Legendre functions, $P_1(\cos\theta)$ and $P_2(\cos\theta)$, defined as

$$P_1(\cos\theta) = \langle\cos\theta\rangle \tag{4}$$

$$P_2(\cos\theta) = \frac{3}{2}\langle\cos^2\theta\rangle - \frac{1}{2} \tag{5}$$

have then been calculated and accumulated as histograms in R with a resolution of 0.1 Å. $P_1(\cos\theta)$ is not particularly interesting as it should normally be zero for all values of R because of the symmetry. It is calculated here simply as a consistency check and to indicate the range of R for which statistically significant results can be obtained. From the results of the simulations, $P_1(\cos\theta)$ is, as expected, very close to zero except for values of R in excess of ∼70 Å where statistics become increasingly poor.

$P_2(\cos\theta)$ is plotted as a function of R in Figure 3. From the definition of $P_2(\cos\theta)$, eq 5, the limiting values are $-1/2$ for a perfectly perpendicular alignment, 1 for perfectly parallel alignment, and 0 for a random alignment of the two vectors defining θ. Clearly in the vicinity of the first peak of $\rho(R)$, ∼23 Å, the chains are very much aligned perpendicular to the outward pointing normal to the interface; i.e., the chains lie very much parallel to the interface. As R increases, there follow oscillations in $P_2(\cos\theta)$ which gradually diminish. At large R the value of $P_2(\cos\theta)$ tends to the random orientation limit of zero. The oscillations are similar to those in seen in $\rho(R)$, and there is clearly a correlation with peaks in

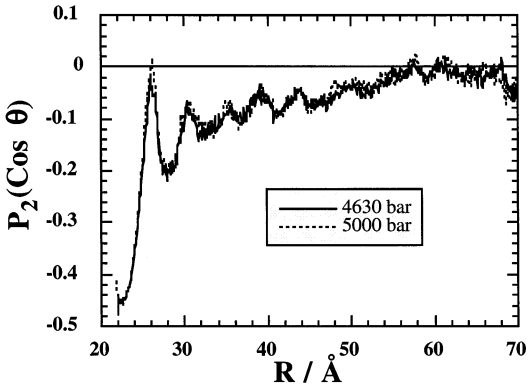

Figure 3. Mean values of $P_2(\cos\theta)$ plotted as a function of R for the composite system at the two pressures shown. θ is the angle between the local polymer chain axis and the outwardly pointing vector normal to the nanoparticle surface. An alignment of the chains parallel to the nanoparticle surface implies a value of $-1/2$ (small R). A random alignment corresponds to a value of zero (large R).

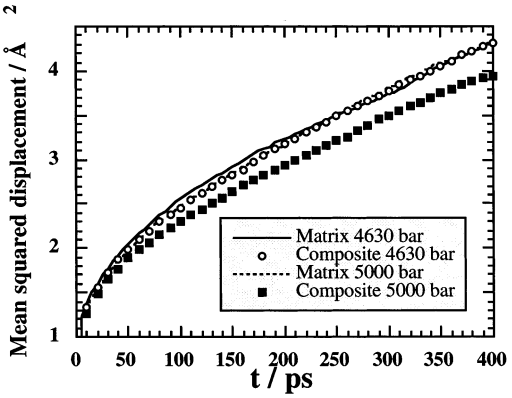

Figure 4. Mean-square displacements of the CH_2 sites in the polymer chains for the simulations shown. Each curve was averaged over all CH_2 sites and over all time origins separated by 5 ps for the period of 500 ps at the end of each production simulation.

mass density corresponding to an alignment of chains more parallel to the interface. Differences between the two different pressures are not particularly marked for this function.

Unlike previous findings for freely jointed chains against plain walls,[27] no tendency toward significant oscillations of $P_2(\cos\theta)$ toward positive values was seen. This is probably due to the more structured (stiffer) chains used in this work and the fact that the angle between the outward normal vector and the bond vectors were used to define θ in ref 27. Other published results for the filler−polymer interface[22] used a definition of θ based on the radial vector and the vector between beads separated by three others along the chains. This, combined with the less structured chains, led to a less oscillatory, though similar, trend from near-parallel alignment of the chains to the interface toward isotropic at longer distances.

The three functions analyzed thus lead to a consistent picture with regard to the structural changes induced in the polymer matrix by the nanoparticle. Chains have a strong tendency to lie parallel to the interface are more likely to be in the *trans* state and thus pack more effectively together, thus leading to a localized peak in the radial mass density. Successive shells then follow where these tendencies gradually diminish toward the pure matrix values. For this particular model system we can say that, as far as static properties are concerned, the interphase is on the order of 30−40 Å thick. In the next section dynamic properties are examined in order to characterize the R dependence of molecular mobility.

3.3. Molecular Mobility. 3.3.1. Mean-Square Displacements. The mean-square displacement, MSD, of a particular atom, i, with respect to a certain time origin, t_o, are calculated in the following way from the trajectory generated in the course of an NPT simulation

$$\Delta r_i^2(t) = (\mathbf{r}_i(t + t_o) - \mathbf{h}(t + t_o)\,\mathbf{h}^{-1}(t_o)\,\mathbf{r}_i(t_o))^2 \quad (6)$$

where $\mathbf{h}$ represents the 3×3 matrix of basis vectors, $\{\mathbf{a}, \mathbf{b}, \mathbf{c}\}$, describing the shape and size of the MD cell. As $\mathbf{h}$ varies with time, the operation in eq 6 avoids including displacements arising simply from changes in the shape and size of the MD box. The average MSDs have been calculated separately for the Si and O atoms and the CH_2 sites for the period covering the last 500 ps of each production simulation and using time origins separated by intervals of 5 ps. The resulting curves for the Si and O atoms (not shown) confirm that they remain close to their initial positions, MSDs < 0.5 Å^2. In fact, this residual motion is consistent with the small changes measured in the position of the center-of-mass of the nanoparticle. The curves for the CH_2 sites are shown in Figure 4. They show an initial rapid rise to $\sim$1 Å^2 in the first few picoseconds and then a gradual leveling off toward a linear increase in time. From this latter diffusive regime the Einstein equation can be used to estimate diffusion coefficients, D,

$$D = \lim_{t\to\infty} \frac{1}{6t}\langle \Delta r_i^2(t)\rangle = \lim_{t\to\infty} \frac{1}{6}\frac{\mathrm{d}\langle \Delta r_i^2(t)\rangle}{\mathrm{d}t} \quad (7)$$

Linear fits to the periods between 200 and 400 ps give estimates for D inferior to 10^{-11} m^2 s^{-1}. We note that, as the pure polymer matrix system only contains one primary chain, the long time diffusion coefficient of individual atoms must be zero; i.e., their mean-square displacements have an upper bound. This arises because the sum of all the forces on the atoms is zero and the sum of all the linear momenta are zero initially, thus fixing the center-of-mass of the chain. This effect will not be seen in the individual CH_2 site displacements until they start to approach values of the order of the mean-square radius of gyration for a chain of this length, i.e., in a time much greater than a few 100 ps. We note briefly in passing that in a separate simulation, where the polymer matrix was cooled from 500 K at -0.1 K/ps, a volumetric T_g at about 170 K was observed, and so a certain amount of mobility is to be expected.

Of the four curves shown in Figure 4, only that for the polymer chains in the composite system at 5000 bar shows any sign of departure from the common behavior of the other three with a slight diminution of the MSD. To try and determine whether this results from an immobilization of the chains close to the interface, MSDs have been calculated as a function of R. For the purpose of accumulating the histograms, CH_2 sites are assigned to regions of R based on their positions with respect to the time origin, t_o, being considered. This makes the accumulation of the MSDs simpler but ultimately leads to some fuzziness in the definition of the (virtual)

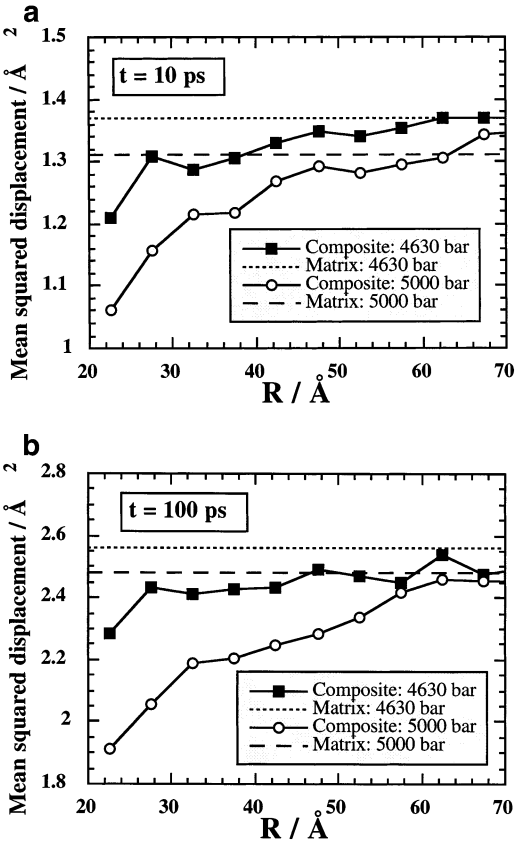

Figure 5. Mean-square displacements of the CH_2 sites in the polymer chains as a function of R at (a) 10 ps and (b) 100 ps. The histograms were accumulated using intervals in R of 5 Å width. Each point was averaged over all CH_2 sites in such concentric shells at a particular time origin. All time origins separated by 5 ps for the period of 500 ps at the end of each production simulation were used. Average MSDs found in the pure matrices at the same times are shown as straight lines.

boundaries between different regions; with time the particles move, and inevitably some will find themselves in other regions than they were at t_o. However, even for a 400 ps time interval the root-mean-square displacement is only ~2 Å and as a resolution of 5 Å is used, in the histograms to be shown, this is not considered to be a big problem.

In parts a and b of Figure 5 the MSDs as a function of R are shown at time intervals of 10 and 100 ps, respectively. For larger time intervals there are fewer time origins available, and the results become subject to larger statistical uncertainties and are not shown. Up to 100 ps though a consistent picture emerges. The mobility of the polymer is reduced close to the interface and increases smoothly the further from it before returning to the pure matrix values, shown as straight lines in Figure 5, within 30−40 Å. This effect is less pronounced for the system at the lower pressure, thus explaining the very similar overall MSDs for the matrix in the composite and the pure matrix (see Figure 4). However, there is a clear sensitivity to the pressure as mobilities close to the interface fall by up to 25% for the system at 5000 bar. Of course, there is a lot less of the polymer close to the nanoparticle than at larger R; e.g., in the region of R between 20 and 25 Å there is about 6 times less CH_2 sites than from 45 to 50 Å, so the net effect on the average MSD (Figure 4) is nothing like as pronounced but sufficient to give the observed difference.

At first sight it seems somewhat surprising that the significant amount of static ordering does not provoke even more immobilization in the layers close to the interface. Also surprising is the result that the mobility at short distances is quite sensitive to the pressure, the static properties being much less so. To try and see whether this trend is peculiar to the MSDs, a second dynamic property has been investigated.

3.3.2. Conformational Correlations. To try and evaluate the possible effects of the presence of the nanoparticle on the *trans*−*gauche* interconversion dynamics of torsional modes, relaxation functions of the form

$$R_{TT}(t) = \langle H_T\{\tau_i(0)\}\, H_T\{\tau_i(t)\}\rangle \qquad (8)$$

were computed. In eq 8, $\tau_i(t)$ is the value of dihedral angle i at time t and $H_T\{\tau_i(t)\}$ is the characteristic function of the *trans* state. $H_T\{\tau_i(t)\}$ takes only two values:

$$H_T\{\tau_i(t)\} = 1 \qquad \text{if } -60° < \tau_i(t) < 60° \qquad (9)$$

and zero otherwise. The method has been presented in detail elsewhere[53] and provides a reliable method for assessing the degree of conformational equilibrium in a system and the rate at which it is attained. The normalized form of the correlation function, $C_{TT}(t)$, is defined as

$$C_{TT}(t) = \frac{R_{TT}(t) - \langle X_T\rangle^2}{\langle X_T\rangle - \langle X_T\rangle^2} \qquad (10)$$

where $\langle X_T\rangle = R_{TT}(0)$ is the mean *trans* fraction.

Figure 6 shows the normalized relaxation functions for the *trans* state of the C−C−C−C backbone torsions in different ranges of R for the composite systems and pure polymer matrices at (a) 4630 bar and (b) 5000 bar. At 4630 bar the $C_{TT}(t)$ in the composite at different values of R are very similar to that found in the pure polymer matrix. At 5000 bar there is an apparent slowing down of the relaxation for those torsions closest to the interface. This is evident in Figure 6b for the range 20−25 Å, but a closer inspection of the data also reveals some slowing down in the range 25−30 Å. These results thus confirm the trend seen with the MSDs, only really at the higher pressure and at low R is there a noticeable immobilization effect. We note in passing that these relaxation functions fit quite well to the KWW stretched exponential form:

$$C_{TT}(t) = \exp(-(t/\tau)^{\beta}) \qquad (11)$$

For example, for the pure matrix at 4630 bar the best fit parameters are $\tau = 174$ ps and $\beta = 0.45$. At 5000 bar the corresponding values are $\tau = 188$ ps and $\beta = 0.46$, there being in fact only a very slight influence of pressure on these relaxation functions for the pure matrices.

A very short-range influence of the interface on mobility has also been found for much shorter model polymer chains against a plain wall.[27] However, a detailed study of the incoherent intermediate scattering function for short polymers in the vicinity of a model nanoparticle using MD techniques has revealed the influence of the strength of the nanoparticle−polymer

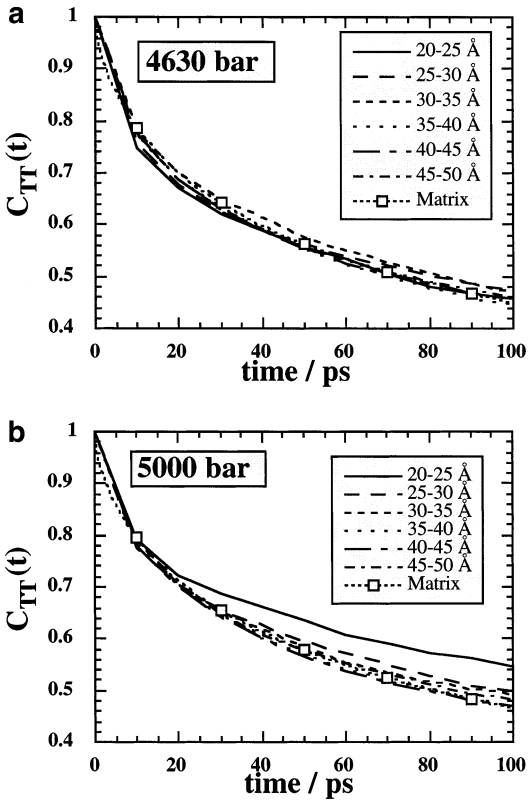

Figure 6. Normalized $C_{TT}(t)$ relaxation functions found in the regimes of R given compared to that in the pure polymer matrix at (a) 4630 bar and (b) 5000 bar. Note that the functions for the pure matrices were evaluated with a resolution of 1 ps whereas those for the composite systems were evaluated at a coarser resolution of 10 ps. This difference is only really visible in the region from 0 to 10 ps.

interaction on the polymer dynamics.[25] Understandably, it was found that strong attractive interactions reduce mobility. Less obvious a finding though was that purely repulsive and even weakly attractive interactions actually enhance mobility, at least under the constant limiting long-range polymer density condition which was applied in the absence of a pressure calculation. Our results show that the gradient of mobility is very sensitive to the applied pressure, and it is not inconceivable that in our model there exists a pressure regime where this enhancement of mobility at the interface may take place also. Our results suggest though that this would have to be at a lower pressure than 4630 bar, i.e., corresponding to a negative pressure regime for the model which included polymer−polymer attractions. The absence of an enhancement in mobility at the interface in our model, which has purely repulsive polymer−nanoparticle interactions, could also be brought about by the manner in which the composite is created or by the mere fact that the chains are substantially longer. Further work would be required though to determine the exact reason(s).

3.4. Bulk Modulus. In this pilot study we have mostly concentrated on the structure and dynamics of the polymer in the vicinity of the silica nanoparticle and have said little about the mechanical properties. This will be the subject of future work using nonequilibrium MD techniques to obtain the stress vs strain response. However, as we have equilibrium data at two different pressures estimates of the bulk moduli can be obtained either from the difference in density ($\Delta\rho$) or volume (ΔV)

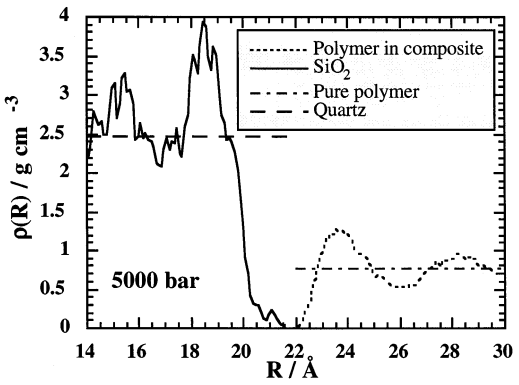

Figure 7. Mass density of the silica particle and the surrounding polymer as a function of R, the distance from the center-of-mass of the silica particle, in the region of the interface for the system equilibrated at a pressure of 5000 bar. The straight dashed line gives the density of the quartz model, and the straight dash−dot line is that determined from the pure polymer matrix simulation.

in combination with the difference in pressure (ΔP) via the approximations

$$K_o \approx \bar{\rho}\frac{\Delta P}{\Delta \rho} \approx -\bar{V}\frac{\Delta P}{\Delta V} \tag{12}$$

where $\bar{\rho}$ is the mean density and $\bar{V}$ is the mean volume. The values obtained using either approximation are about the same and give for the matrix and the composite 3.7 ± 0.1 and 3.4 ± 0.1 GPa, respectively. In effect, the inclusion of the SiO_2 particle leads to a slight reduction of the bulk modulus; i.e., it increases the compressibility of the system as a whole. In other words, the change in volume of the MD box (see Table 3) is greater in the case of the composite: 10630 Å^3 compared to 9134 Å^3 in the pure matrix. As this is somewhat contrary to the usual reinforcement behavior of such composite materials, further investigations have been carried out to try and uncover the origin of this effect.

To do this, we have examined the radial mass density functions for the composite systems in the interfacial region. The plot for the data at 5000 bar is shown in Figure 7; the full range of $\rho(R)$ for the polymer is already shown in Figure 1, and the $\rho(R)$ for the SiO_2 at the lower pressure is almost identical to that at 5000 bar. Figure 1 shows that in this model system the interface is rather well-defined with virtually no interpenetration. The radial density of the SiO_2 oscillates around the value for the quartz model before falling sharply at ∼20 Å. We have verified that the slight tail in the function is almost entirely due to oxygen atoms, as would be expected from the silicon ions preferring to rest coordinated to four oxygens. At both pressures the radius at which the SiO_2 density goes to zero and the polymer density starts is about the same, ∼21.7 Å. The two components are seen to mutually exclude themselves from a zone of about ∼2 Å width. Indeed, if we calculate the expected volume of the composite from the respective densities of the quartz and the pure polymer, there is a difference in volume of 8801 and 7305 Å^3 at 4630 and 5000 bar, respectively. This nonadditivity of volume is largely due to the form adopted for the nanoparticle−polymer interaction, purely repulsive, and is not of any major consequence. More interesting is the difference in compressibility of the polymer component between the pure phase and the composite.

We note first that the apparent invariance of the size of the nanoparticle with pressure is consistent with what would be expected on the basis of eq 12 and the bulk modulus of the quartz model, $K_o \sim 32$ GPa. The expected change in volume of the nanoparticle, V_n, for a pressure increase of 370 bar, $\Delta V_n = -V_n \Delta P/K$, is only a decrease of about 50 Å^3. This corresponds to a less than 0.01 Å reduction in the radius of the nanoparticle, i.e., less than the resolution of the presented histograms. To a very good approximation, for the level of pressure differential applied, the volume change in the composite system can be considered to take place purely in the polymer matrix. If we use the total difference in volume for the composite system, ΔV, and the average volume deemed to be occupied by the polymer, $\bar{V}_p$, to determine a nominal bulk modulus for the polymer part of the composite, $K_p = -\bar{V}_p \Delta P/\Delta V$, a value of ~3.2 GPa is obtained, i.e., significantly less than the pure polymer value. This calculation assumes that all the polymer is affected equally whereas we know from the mass density distributions that there is an obvious dependence on R. The difference between the mass density distributions, $\Delta\rho(R)$, of the polymer in the composite at the two pressures, in principle, contains all the necessary information concerning the radial resolution of the polymer compressibility but this function (not shown) at a 0.1 Å resolution is highly oscillatory. Instead, we have first used the following equation

$$\overline{\Delta\rho}(R_1,R_2) = \frac{\int_{R_1}^{R_2} \Delta\rho(R)\, 4\pi R^2\, \mathrm{d}R}{\frac{4\pi(R_2^3 - R_1^3)}{3}} \qquad (13)$$

to obtain the changes in mass density in regions of R defined by the limits R_1 and R_2. The results depend somewhat on the (arbitrary) choice of interval, but there is confirmation that in the region up to $R = 40$ Å the change in density is greater than that in the region from $R = 40-50$ Å, this latter region having a change in density much more like that found in the pure polymer matrix.

An alternative, though nonrigorous, approach is to fit the $\Delta\rho(R)$ to a smooth function, $\Delta\rho_s(R)$, and then obtain a corresponding smooth approximation to the radial dependent bulk modulus from

$$K_s(R) = \bar{\rho}(R)\Delta P/\Delta\rho_s(R) \qquad (14)$$

We note in passing that a more rigorous approach to this kind of problem might be possible using density functional theory.[54,55] Although such techniques have been applied to equilibrium melts of short chains of hard particles at interfaces,[55] we have not explored this avenue for our system with its very long "soft" chain. Nor have we tried to use definitions of atomically local bulk modulus[56] which may also be a possibility although it is even further removed from the comparison we would like to make with continuum mechanics.

For eq 14, the size of the oscillations in $\Delta\rho(R)$ itself make it difficult to justify a fit to a particular functional form. As a first approximation, a linear function can be used for $\Delta\rho_s(R)$, but as this simple form does not have the right asymptotic behavior, we have preferred to fit to the following $1/R$ form

$$\Delta\rho_s(R) = \lambda/(R - R_0) + \Delta\rho_m \qquad (15)$$

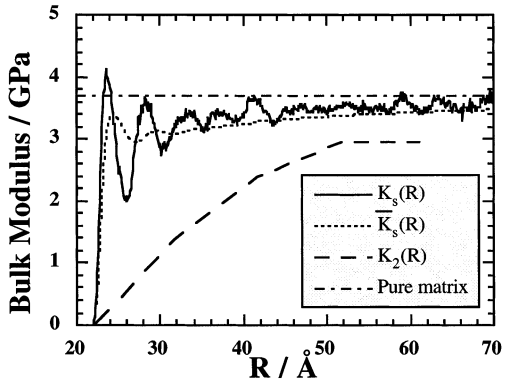

Figure 8. Smooth approximation to the radial dependent bulk modulus $K_s(R)$ for the interphase region of the polymer matrix as determined from eq 14. Also shown is the mass-weighted running average of this function, $\bar{K}_s(R)$, and the corresponding bulk modulus based on the micromechanical calculations, $K_2(R)$.

where λ and R_0 are the adjustable parameters and $\Delta\rho_m$ is the limiting value for the difference in density of the polymer matrix at the two pressures, i.e., 7.6 kg m^{-3} in this case. By fixing R_0 at 20 Å, a best fit value to the data for $\Delta\rho(R)$ gives $\lambda = 13.6$ kg m^{-3} Å. The corresponding smoothed bulk modulus function (eq 14) is shown in Figure 8. Necessarily, it contains the oscillations associated with the radial density function.

Although this approximate approach is useful for our purpose of characterizing the radial dependence of the bulk modulus, we make a note of caution regarding the equating of the change in density in a spherical shell directly to K (eq 14). Continuum mechanical approaches have been developed to predict the elastic moduli of composite systems where spherical particles are embedded in polymer matrices, and these give rise to more rigorous relationships. It is interesting and instructive to apply these micromechanical modeling techniques to this case even though we know from the analyses already made that the underlying assumptions of isotropy and homogeneity, generally used in continuum mechanics, are not strictly valid.

In the treatment of Hervé and Zaoui,[38] for example, the composite can be considered as a series of concentric spheres with each successive shell representing a different component, or phase, of the composite. Assuming each phase to be isotropic and homogeneous with perfect bonding between neighboring phases, the effective bulk modulus of the n-phase model can be expressed using the following recursive relation

$$K_n^{\mathrm{eff}} = K_n + \frac{R_{n-1}^3(K_{n-1}^{\mathrm{eff}} - K_n)(3K_n + 4G_n)}{R_n^3(3K_n + 4G_n) + 3(R_n^3 - R_{n-1}^3)(K_{n-1}^{\mathrm{eff}} - K_n)} \qquad (16)$$

with R_n, G_n, and K_n the radius, shear modulus, and bulk modulus, respectively, of the nth phase and $K_1^{\mathrm{eff}} = K_1$. In the case in question a three-phase model is a reasonable first approximation. The nanoparticle forms the hard inner core, phase 1. This is surrounded by a layer of modified polymer, phase 2, which forms the "interphase" between the nanoparticle and the third phase, the unperturbed polymer matrix. For the three-

phase model it has been shown[38] that the overall bulk modulus can be written as

$$K = K_3 + \{R_2^3(3K_3 + 4G_3)[R_1^3(K_1 - K_2) \times (3K_3 + 4G_2) + R_2^3(K_2 - K_3)(3K_1 + 4G_2)]\}/\{3R_1^3(K_2 - K_1)[R_2^3(3K_3 + 4G_2) + 4R_3^3(G_3 - G_2)] + R_2^3(3K_1 + 4G_2)[3R_2^3(K_3 - K_2) + R_3^3(3K_2 + 4G_3)]\} \quad (17)$$

From the MD simulations, we have already the radius of the nanoparticle and the bulk moduli of the models of the composite, the pure silica, and the pure polymer matrix. Estimates of the shear modulus can be obtained from these bulk moduli and estimates, either simulated or experimental, of Poisson's ratio, but in any case, the results are relatively insensitive to the shear moduli. Equation 17 can then be inverted[15,57] in order to obtain an estimate of the interphase bulk modulus, K_2, within the approximations of this continuum mechanics model. The results of such calculations are also shown in Figure 8 as the dashed line marked $K_2(R)$. This is the average bulk modulus required of an isotropic and homogeneous interphase of thickness $R - R_1$. Also given in Figure 8 is the mass-weighted average value of the smoothed bulk modulus, $\bar{K}_s(R)$. This latter function represents the average value of $K_s(R)$ for the region between R_1 and R and thus provides a direct comparison with $K_2(R)$. For $R_2 \sim 60$ Å, i.e., an interphase thickness of ~40 Å, it would seem that the three-phase continuum mechanics model underestimates the average bulk modulus in the interphase region: ~3 GPa compared to ~3.5 GPa for $\bar{K}_s(R_2)$. Given the approximations necessary in order to determine $K_s(R)$ from the MD results, this remains a fairly tentative conclusion albeit not unreasonable given the obvious departure from isotropy and homogeneity.

On the basis of this apparent thickness of the interphase region, further continuum mechanics calculations have been made in order to see the effect of increasing the size of the particle while keeping the volume fraction of filler and the thickness of the modified polymer layer constant. Under these conditions the volume fraction of the interphase falls rapidly as $1/R$, and a reinforcement effect is recovered for radii above ~100 Å. Although we have not yet attempted to determine the dependence of the interphase thickness for particles of greater size by MD simulation, previous results using similar models at planar interfaces[27] and scaling arguments[58] suggest strongly that it will not change significantly.

4. Conclusion

The feasibility of performing atomistic level simulations of nanoparticles embedded in polymer matrices has been demonstrated. Sufficient statistics can be gathered to enable static and dynamic properties to be determined as a function of the distance from the interface. This is encouraging for the next stage of our project where more specific models are currently being investigated for comparison with actual experimental composite systems. It is important to remember that in this model the polymer−polymer and polymer−nanoparticle interactions are completely repulsive. The "missing" attractive interactions are, of course, compensated by the applied overpressures. The model can thus be considered as just one limit where polymer−nanoparticle attractions are at their weakest. Nevertheless, it is seen that the structural ordering is quite significant. Dynamic effects are less obvious, but some clue as to their sensitivity to the strength of the polymer−nanoparticle interaction can be seen in the way that they increase significantly with the applied overpressure. In a qualitative way this decrease in mobility is likely to be similar to that which would be provoked by including attraction between the polymer and the nanoparticle. With respect to real experiments, these simulation results suggest the "thickness" of the interphase is sensitive to the property investigated.

In this particular model, where the very small size of the inclusions gives rise to a high volume fraction of interphase, the disruption of the polymer matrix in the interphase region leads to a bulk modulus of the composite lower than that of the pure polymer matrix. Whether this kind of softening effect could ever be seen in reality is debatable. Preparing real systems with significant volume fractions of silica presents an ongoing challenge to the experimentalist. Thermodynamically, the dispersion of such small particles would not be favorable as it maximizes the disturbance of the preferred structure of the polymer matrix. Indeed, the likelihood is that silica particles would be obliged to cluster together by such a thermodynamic force once volume fractions of silica became significant. It is, however, not impossible that a method could be developed which bypasses such dispersion problems though whether one would want to produce softened composites is another matter.

Finally, the question arises as to whether the results presented here will be generally the case as particle size decreases. We do not discount the possibility that in other cases the interactions between the inclusion and the matrix could lead to an interphase with a higher bulk modulus and thus rather enhanced reinforcement properties. This is subject of work currently under way, and the results will be published in due course.

Acknowledgment. The IDRIS (Orsay, France) and the CINES (Montpellier, France) computer centers are acknowledged for the provision of computer time on the Cray T3E and on the SGi O2000. The Rhône-Alpes Region and the University of Savoie are thanked for financing the acquisition of a COMPAQ DS20E biprocessor server.

References and Notes

(1) Boluk, M. Y.; Schreiber, H. P. *Polym. Compos.* **1986**, *7*, 295−301.
(2) Mélé, P.; Albérola, N. D. *Polym. Compos.* **1996**, *17*, 749−759.
(3) Vidal, A.; Donnet, J. B. *Prog. Colloid Polym. Sci.* **1987**, *75*, 201−212.
(4) Tsagaropoulos, G.; Eisenberg, A. *Macromolecules* **1995**, *28*, 396−398.
(5) Tsagaropoulos, G.; Eisenberg, A. *Macromolecules* **1995**, *28*, 6067−6077.
(6) Haidar, B.; Salah Deradji, H.; Vidal, A.; Papirer, E. *Macromol. Symp.* **1996**, *108*, 147−162.
(7) Ou, Y. C.; Yu, Z. Z.; Vidal, A.; Donnet, J. B. *J. Appl. Polym. Sci.* **1996**, *59*, 1321−1328.
(8) Vidal, A.; Haidar, B. *Lebanese Sci. Res. Rep.* **1997**, *2*, 54−60.
(9) Albérola, N. D.; Fernagut, F.; Mélé, P. *J. Appl. Polym. Sci.* **1997**, *63*, 1029−1040.
(10) Sumita, M.; Ookuma, T.; Miyasaka, K.; Ishikawa, K. *J. Mater. Sci.* **1982**, *17*, 2869−2877.
(11) Sumita, M.; Tsukihi, H.; Miyasaka, K.; Ishikawa, K. *J. Appl. Polym. Sci.* **1984**, *29*, 1523−1530.

(12) Datta, S.; De, S. K.; Kontos, E. G.; Wefer, J. M.; Wagner, P.; Vidal, A. *Polymer* **1996**, *37*, 3431−3435.
(13) Datta, S.; Bhattacharya, A. K.; De, S. K.; Kontos, E. G.; Wefer, J. M. *Polymer* **1996**, *37*, 2581−2586.
(14) Albérola, N. D.; Benzarti, K. *C. R. Acad. Sci., Ser. IIb* **1997**, *325*, 249−255.
(15) Vendramini, J.; Mélé, P.; Merle, G.; Albérola, N. D. *J. Appl. Polym. Sci.* **2000**, *77*, 2513−2524.
(16) Gong, X.; Hine, P. J.; Duckett, R. A.; Ward, I. M. *Polym. Compos.* **1994**, *15*, 74−82.
(17) Chevalier, Y.; Hidalgo, M.; Cavaillé, J.-Y.; Cabane, B. *Macromolecules* **1999**, *32*, 7887−7896.
(18) Hajji, P.; David, L.; Gerard, J. F.; Pascault, J. P.; Vigier, G. *J. Polym. Sci., Part B: Polym. Phys.* **1999**, *37*, 3172−3187.
(19) Favier, V.; Canova, G. R.; Shrivastava, S. C.; Cavaille, J. Y. *Polym. Eng. Sci.* **1997**, *37*, 1732−1739.
(20) Dutta, N. K.; Roy Choudhury, N.; Haidar, B.; Vidal, A.; Donnet, J. B. *Polymer* **1994**, *35*, 4293−4299.
(21) Mansencal, R.; Haidar, B.; Vidal, A.; Delmotte, L.; Chezeau, J.-M. *Polym. Int.* **2001**, *50*, 387−394.
(22) Vacatello, M. *Macromolecules* **2001**, *34*, 1946−1952.
(23) Vacatello, M. *Macromol. Theory Simul.* **2002**, *11*, 501−512.
(24) Starr, F. W.; Schrøder, T. B.; Glotzer, S. C. *Phys. Rev. E* **2001**, *64*, 021802.
(25) Starr, F. W.; Schrøder, T. B.; Glotzer, S. C. *Macromolecules* **2002**, *35*, 4481−4492.
(26) Kasemagi, H.; Klintenberg, M.; Aabloo, A.; Thomas, J.-O. *J. Mater. Chem.* **2001**, *11*, 3191−3196.
(27) Bitsanis, I.; Hadziioannou, G. *J. Chem. Phys.* **1990**, *92*, 3827−3847.
(28) Baschnagel, J.; Binder, K. *Macromolecules* **1995**, *28*, 6808−6818.
(29) Baschnagel, J.; Binder, K. *J. Phys., I* **1996**, *6*, 1271−1294.
(30) Baschnagel, J.; Binder, K. *Macromol. Theory Simul.* **1996**, *5*, 417−448.
(31) Tej, M. K.; Meredith, J. C. *J. Chem. Phys.* **2002**, *117*, 5443−5451.
(32) Brown, D.; Minoux, H.; Maigret, B. *Comput. Phys. Commun.* **1997**, *103*, 170−186.
(33) Brown, D.; Maigret, B. *Speedup* **1999**, *12*, 33−40.
(34) Brown, D. The *gmq* User Manual, version 3, 1999.
(35) Brown, D.; Clarke, J. H. R.; Okuda, M.; Yamazaki, T. *J. Chem. Phys.* **1994**, *100*, 6011−6018.
(36) Neyertz, S.; Brown, D. *J. Chem. Phys.* **2001**, *115*, 708.
(37) Hashin, Z. *J. Mech. Phys. Solids* **1991**, *39*, 745−762.
(38) Hervé, E.; Zaoui, A. *Int. J. Eng. Sci.* **1993**, *31*, 1−9.
(39) Nakano, A.; Bi, L. S.; Kalia, R. K.; Vashishta, P. *Phys. Rev. B: Condens. Matter* **1994**, *49*, 9441−9452.
(40) Tsuneyuki, S. *Mol. Eng.* **1996**, *6*, 157.
(41) Berendsen, H. J. C.; Postma, J. P. M.; van Gunsteren, W. F.; DiNola, A.; Haak, J. R. *J. Chem. Phys.* **1984**, *81*, 3684−3690.
(42) Brown, D.; Clarke, J. H. R. *Comput. Phys. Commun.* **1991**, *62*, 360−369.
(43) Fincham, D. *Inf. Q. Comput. Simul. Condens. Phases* **1993**, *38*, 17−24.
(44) Brown, D.; Neyertz, S. *Mol. Phys.* **1995**, *84*, 577−595.
(45) Levien, L.; Prewitt, C. T.; Weidner, D. J. *Am. Mineral.* **1980**, *65*, 920−930.
(46) Brown, D.; Clarke, J. H. R. *Macromolecules* **1991**, *24*, 2075−2082.
(47) Brown, D.; Clarke, J. H. R.; Okuda, M.; Yamazaki, T. *J. Chem. Phys.* **1994**, *100*, 1684−1692.
(48) Brown, D.; Clarke, J. H. R.; Okuda, M.; Yamazaki, T. *J. Chem. Phys.* **1996**, *104*, 2078−2082.
(49) Sharaf, M. A.; Kloczkowski, A.; Mark, J. E. *Comput. Theor. Polym. Sci.* **2001**, *11*, 251−262.
(50) Vacatello, M. *Macromolecules* **2002**, *35*, 8191−8193.
(51) Roulstone, B. J.; Wilkinson, M. C.; Hearn, J.; Wilson, A. J. *Polym. Int.* **1991**, *24*, 87−94.
(52) Wang, Y.; Juhué, D.; Winnik, M. A.; Leung, O. M.; Goh, M. C. *Langmuir* **1992**, *8*, 760−762.
(53) Brown, D.; Clarke, J. H. R. *J. Chem. Phys.* **1990**, *92*, 3062−3073.
(54) Tarazona, P. *Phys. Rev. A* **1985**, *31*, 2672−2679.
(55) Yethiraj, A. *Chem. Eng. J.* **1999**, *74*, 109−115.
(56) Kelires, P. C. *Phys. Rev. B* **2000**, *62*, 15686−15694.
(57) Albérola, N. D.; Benzarti, K. *Polym. Eng. Sci.* **1998**, *38*, 429−439.
(58) de Gennes, P.-G. *Scaling Concepts in Polymer Physics*; Cornell University Press: Ithaca, NY, 1979.

MA020951S